Space-Time-Frequency Characterization of Non-Isotropic MIMO Mobile-to-Mobile Multicarrier Ricean Fading Channels

Xiang Cheng*, Cheng-Xiang Wang*, David I. Laurenson**, Hsiao-Hwa Chen†, and Athanasios V. Vasilakos††
*Joint Research Institute for Signal and Image Processing, Heriot-Watt University, EH14 4AS, Edinburgh, UK.
**Joint Research Institute for Signal and Image Processing, University of Edinburgh, EH9 3JL, Edinburgh, UK.
†Department of Engineering Science, National Cheng Kung University, Taiwan, No.1, University Road, Tainan City 701, Taiwan.
††Department of Computer and Telecommunications Engineering, University of Western Macedonia, GR 50100 Kozani, Greece.
Email: xc48@hw.ac.uk, cheng-xiang.wang@hw.ac.uk, dave.laurenson@ed.ac.uk, hshwchen@ieee.org, vasilako@ath.forthnet.gr

***Abstract*—This paper proposes a new space-time-frequency (STF) correlation model based on the two-ring model with both single- and double-bounced rays for miltiple-input multiple-output (MIMO) mobile-to-mobile (M2M) multicarrier Ricean fading channels in a non-isotropic scattering environment. The proposed model allows us to study the correlation functions (CFs) between any two sub-channels with different carrier frequencies of MIMO M2M Ricean fading channels. The derived STF CF and the corresponding space-Doppler-frequency (SDF) power spectral density (PSD) have generic closed-form expressions including many existing CFs and PSDs as special cases. Based on the derived SDF PSD, the resulting Doppler PSD is investigated in more detail in terms of some important parameters. Our numerical evaluations show the impacts of different parameters of the propagation environment on the Doppler PSD. More importantly, we find that the shapes of the Doppler PSD are completely different according to single- or double-bounced rays for M2M channels, while they are exactly the same for fixed-to-mobile (F2M) channels. Finally, it is worth mentioning that some interesting observations obtained from these numerical results can be considered as the guidance for further proposing more realistic M2M channel models and building up future measurement campaigns.**

I. Introduction

Recently, M2M communications have received much attention due to some new applications, such as wireless mobile ad hoc networks, relay-based cellular networks, intelligent transportation systems, and dedicated short range communications (DSRC) systems, where both the transmitter (Tx) and receiver (Rx) are in motion and equipped with low elevation antennas. Such M2M communication systems differ from conventional fixed-to-mobile (F2M) cellular radio systems, where only one terminal (mobile station) is moving while the other one (base station) is fixed. Therefore, many existing channel models developed solely for conventional cellular radio systems can not directly be used for M2M communication systems. Akki and Haber [1], [2] were the first to propose a channel model for single-input single-output (SISO) M2M Rayleigh fading channels and further investigate the corresponding statistical properties. Recently, two-ring geometrical stochastic models considering only double-bounced rays for MIMO M2M Rayleigh fading channels were presented in [3] and [4] for isotropic and non-isotropic scattering environments, respectively. In [5], the authors proposed a more general two-ring model for MIMO M2M channels taking into account the line-of-sight (LoS), single-, and double-bounced rays, but they did not further study the difference between the single- and double-bounced rays. However, all the aforementioned MIMO M2M channel models only investigated space-time (ST) correlation properties of MIMO M2M channels. Frequency correlation properties of two narrowband sub-channels [6] in a MIMO M2M channel have not been studied so far. Moreover, although the Doppler PSD is one of the most important statistical properties that make M2M channels significantly different from F2M channels, more detailed investigations of the Doppler PSD in non-isotropic scattering environments are surprisingly lacking in the open literature.

Motivated by the above gaps, our objectives are mainly two-fold. First, we propose a new STF correlation model based on the two-ring model considering the LoS, single-, and double-bounced rays for MIMO M2M multicarrier Ricean fading channels in non-isotropic scattering environments. Closed-form expressions are derived for the STF CF and the corresponding SDF PSD between any two narrowband sub-channels with different carrier frequencies. As we will see later on, the derived STF CF and SDF PSD include many existing CFs and PSDs as special cases, e.g., those in [3]–[5]. Furthermore, the derived STF CF and SDF PSD are very useful for realistic performance evaluation and comprehensive understanding of MIMO M2M multicarrier systems, e.g., MIMO-orthogonal frequency-division multiplexing (MIMO-OFDM) systems. Second, based on the derived SDF PSD we study in more detail the Doppler PSD in a non-isotropic scattering environment in terms of some important parameters, e.g., the single-/double-bounced rays, mean values of the angle of arrival (AoA) and angle of departure (AoD), angle spreads, antenna element spacings, directions of motion, and frequency separations. More importantly, we find that the contributions to the Doppler PSD from single- and double-bounced rays are not similar anymore in M2M channels, while this is true in F2M cellular channels. Some interesting observations and useful conclusions are obtained which can be considered as the guidance for proposing more realistic MIMO M2M channel

978-1-4244-2202-9/08/$25.00 © 2008 IEEE

models (e.g., the one in [7]) and setting up future M2M channel measurement campaigns.

The paper is structured as follows. In Section II, we introduce the two-ring channel model with the LoS, single-, and double-bounced components for MIMO M2M Ricean fading channels. In Section III, the STF CF and the corresponding SDF PSD of any two sub-channels with different carrier frequencies are derived in a non-isotropic scattering environment. Numerical results and analysis are presented in Section IV. Finally, conclusions are drawn in Section V.

II. Theoretical Model for MIMO M2M Channels

Let us now consider a narrowband single-user MIMO M2M multicarrier communication system with M_T transmit and M_R receive omnidirectional antenna elements. Both the Tx and Rx are in motion and equipped with low elevation antennas. The propagation scenario is characterized by non-isotropic scattering with possibly a LoS component between the Tx and Rx. The MIMO fading channel can be described by an $M_R \times M_T$ matrix $\mathbf{H}(t) = [h_{ij}(t)]_{M_R \times M_T}$ of complex faded envelopes, where $h_{ij}(t)$ denotes the complex impulse response between the jth Tx and the ith Rx.

Fig. 1 illustrates the geometry of a two-ring MIMO M2M channel model, where the LoS, single-, and double-bounced rays are considered. We assume that uniform linear antenna arrays are used with arbitrary numbers of antenna elements. As an example, $M_T = M_R = 2$ were taken in Fig. 1. The two-ring model defines two rings of effective scatterers, one around the Tx and the other around the Rx. Suppose there are N_1 effective scatterers around the Tx lying on a ring of radius R_T and the n_1th ($n_1 = 1, ..., N_1$) effective transmit scatterer is denoted by $S_T^{(n_1)}$. Similarly, assume there are N_2 effective scatterers around the Rx lying on a ring of radius R_R and the n_2th ($n_2 = 1, ..., N_2$) effective receive scatterer is denoted by $S_R^{(n_2)}$. The distance between the Tx and Rx is D. The antenna element spacings at the Tx and Rx are designated by δ_T and δ_R, respectively. It is normally assumed that the radii R_T and R_R are both much larger than the antenna element spacings δ_T and δ_R, i.e., $\min\{R_T, R_R\} >> \max\{\delta_T, \delta_R\}$. The multi-element antenna tilt angles are denoted by β_T and β_R. The Tx and Rx move with speeds υ_T and υ_R in directions determined by the angles of motion γ_T and γ_R, respectively. The symbol $\phi_{R_q}^{LoS}$ denotes the AoA of a LoS path. The AoAs of the waves travelling from the effective scatterers $S_T^{(n_1)}$ and $S_R^{(n_2)}$ towards the Rx are denoted by $\phi_R^{(n_1)}$ and $\phi_R^{(n_2)}$, respectively. The AoDs of the waves that impinge on the effective scatterers $S_T^{(n_1)}$ and $S_R^{(n_2)}$ are designated by $\phi_T^{(n_1)}$ and $\phi_T^{(n_2)}$, respectively.

From the above described geometrical-based model, the received complex impulse response at the carrier frequency f_c for the $T_p - R_q$ link is a superposition of the LoS, single-, and double-bounced rays, and can be expressed as [5]

$$h_{pq}(t) = h_{pq}^{LoS}(t) + h_{pq}^{SB}(t) + h_{pq}^{DB}(t) \tag{1}$$

where

$$h_{pq}^{LoS}(t) = \sqrt{\frac{K_{pq}\Omega_{pq}}{K_{pq}+1}} e^{-j2\pi f_c \tau_{pq}} \times e^{j\left[2\pi f_{T_{max}} t \cos\left(\pi - \phi_{R_q}^{LoS} + \gamma_T\right) + 2\pi f_{R_{max}} t \cos\left(\phi_{R_q}^{LoS} - \gamma_R\right)\right]} \tag{2}$$

$$h_{pq}^{SB}(t) = \sum_{i=1}^{2} h_{pq}^{SB_i}(t) = \sum_{i=1}^{2} \sqrt{\frac{\eta_{SB_i}\Omega_{pq}}{K_{pq}+1}} \lim_{N_1 \to \infty} \sum_{n_1=1}^{N_1} \frac{1}{\sqrt{N_1}} e^{j\left(\psi_{n_i} - 2\pi f_c \tau_{pq,n_i}\right)} \times e^{j\left[2\pi f_{T_{max}} t \cos\left(\phi_T^{(n_i)} - \gamma_T\right) + 2\pi f_{R_{max}} t \cos\left(\phi_R^{(n_i)} - \gamma_R\right)\right]} \tag{3}$$

$$h_{pq}^{DB}(t) = \sqrt{\frac{\eta_{DB}\Omega_{pq}}{K_{pq}+1}} \lim_{N_1, N_2 \to \infty} \sum_{n_1, n_2 = 1}^{N_1, N_2} \frac{1}{\sqrt{N_1 N_2}} \times e^{j\left(\psi_{n_1,n_2} - 2\pi f_c \tau_{pq,n_1,n_2}\right)} \times e^{j\left[2\pi f_{T_{max}} t \cos\left(\phi_T^{(n_1)} - \gamma_T\right) + 2\pi f_{R_{max}} t \cos\left(\phi_R^{(n_2)} - \gamma_R\right)\right]}. \tag{4}$$

In (2)–(4), $p = 1, 2, ..., M_T$, $q = 1, 2, ..., M_R$, $\tau_{pq} = \epsilon_{pq}/c$, $\tau_{pq,n_i} = (\epsilon_{pn_i} + \epsilon_{n_i q})/c$, $\tau_{pq,n_1,n_2} = (\epsilon_{pn_1} + \epsilon_{n_1 n_2} + \epsilon_{n_2 q})/c$ are the travel times of the waves through the link $T_p - R_q$, $T_p - S_T^{(n_1)}$ ($S_R^{(n_2)}$ or $S_{TR}^{(n_3)}$)$-R_q$, and $T_p - S_T^{(n_1)} - S_R^{(n_2)} - R_q$, respectively, with c denoting the speed of light. The symbol K_{pq} designates the Ricean factor of the $T_p - R_q$ link and Ω_{pq} denotes the total power transferred through the $T_p - R_q$ link. Parameters η_{SB_i} and η_{DB} specify how much the single-bounced and double-bounced rays contribute to the total scattered power $\Omega_{pq}/(K_{pq}+1)$. This indicates that these energy-related parameters satisfy $\sum_{i=1}^{2} \eta_{SB_i} + \eta_{DB} = 1$. The phases ψ_{n_i} and ψ_{n_1,n_2} are independent and identically distributed (i.i.d.) random variables with uniform distributions over $[-\pi, \pi)$, $f_{T_{max}} = \upsilon_T/\lambda$ and $f_{R_{max}} = \upsilon_R/\lambda$ are the maximum Doppler frequencies associated with the Tx and Rx, respectively, and λ is the carrier wavelength.

Distances ϵ_{pq}, ϵ_{pn_i}, $\epsilon_{n_i q}$, and $\epsilon_{n_1 n_2}$ in (1)–(4) can be expressed as functions of the relevant angles, e.g., $\phi_{R_q}^{LoS}$, $\phi_T^{(n_i)}$, and $\phi_R^{(n_i)}$. From Fig. 1, assuming $D \gg \max\{\delta_T, \delta_R\}$ and invoking the laws of sines and cosines, these distances are

$$\epsilon_{pq} \approx \epsilon - k_q \delta_R \cos\left(\phi_{R_q}^{LoS} - \beta_R\right) \tag{5}$$

$$\epsilon_{pn_1} \approx R_T - k_p \delta_T \cos\left(\phi_T^{(n_1)} - \beta_T\right) \tag{6}$$

$$\epsilon_{n_1 q} \approx \xi_{n_1} - k_q \delta_R \cos\left(\phi_R^{(n_1)} - \beta_R\right) \tag{7}$$

$$\epsilon_{pn_2} \approx \xi_{n_2} - k_p \delta_T \cos\left(\phi_T^{(n_2)} - \beta_T\right) \tag{8}$$

$$\epsilon_{n_2 q} \approx R_R - k_q \delta_R \cos\left(\phi_R^{(n_2)} - \beta_R\right) \tag{9}$$

$$\epsilon_{n_1 n_2} \approx D - R_T \cos\phi_T^{(n_1)} + R_R \cos\phi_R^{(n_2)} \approx D \tag{10}$$

where $k_p = M_T - 2p + 1/2$, $k_q = M_R - 2q + 1/2$, $\epsilon \approx D - k_p \delta_T \cos\beta_T$, $\phi_{R_q}^{LoS} \approx \pi$, $\xi_{n_1} \approx D - R_T \cos\phi_T^{(n_1)}$, $\phi_R^{(n_1)} \approx \pi - \Delta_T \sin\phi_T^{(n_1)}$, $\xi_{n_2} \approx D + R_R \cos\phi_R^{(n_2)}$, and $\phi_T^{(n_2)} \approx \Delta_R \sin\phi_R^{(n_2)}$ with $\Delta_T \approx R_T/D$ and $\Delta_R \approx R_R/D$.

In this paper, to characterize the AoD $\phi_T^{(n_i)}$ and AoA $\phi_R^{(n_i)}$, we use the von Mises probability density function (PDF) [8] defined as $f(\phi) \triangleq \exp[k\cos(\phi-\mu)]/2\pi I_0(k)$, where $\phi \in [-\pi,\pi)$, $I_0(\cdot)$ is the zeroth-order modified Bessel function of the first kind, $\mu \in [-\pi,\pi)$ accounts for the mean value of the angle ϕ, and k ($k \geq 0$) is a real-valued parameter that controls the angle spread of the angle ϕ. For $k=0$ (isotropic scattering), the von Mises PDF reduces to the uniform distribution, while for $k>0$ (non-isotropic scattering), the von Mises PDF approximates different distributions depending on different values of k.

III. New STF CF and SDF PSD

In this section, based on the two-ring channel model in (1)–(4), we will derive the STF CF and the corresponding SDF PSD of any two narrowband sub-channels with different carrier frequencies in a non-isotropic scattering environment. We also show that the newly derived STF CF includes many existing CFs, e.g., those in [3]– [5], as special cases.

A. New Generic STF CF

The normalized STF CF between any two complex impulse responses $h_{pq}(t)$ and $h_{p'q'}^{(\dagger)}(t)$ with different carrier frequencies f_c and $f_c^{(\dagger)}$, respectively, is defined as

$$\rho_{h_{pq}h_{p'q'}^{(\dagger)}}(\tau,\chi) = \frac{\mathbf{E}\left[h_{pq}(t)\,h_{p'q'}^{(\dagger)*}(t+\tau)\right]}{\sqrt{\mathbf{E}\left[\left|h_{pq}(t)\right|^2\right]\mathbf{E}\left[\left|h_{p'q'}^{(\dagger)}(t)\right|^2\right]}} \tag{11}$$

where $(\cdot)^*$ denotes the complex conjugate operation, $\mathbf{E}[\cdot]$ is the statistical expectation operator, $p,p' \in \{1,2,...,M_T\}$, and $q,q' \in \{1,2,...,M_R\}$. It should be observed that (11) is a function of time separation τ, antenna element spacings δ_T and δ_R, and frequency separation $\chi = f_c^{(\dagger)} - f_c$.

Using (2), (5), and (11), the STF CF of the LoS component can be obtained as

$$\rho_{h_{pq}^{LoS}h_{p'q'}^{LoS(\dagger)}}(\tau,\chi) = \sqrt{K_{pq}K_{p'q'}}e^{j2\pi X - j2\pi\tau Y + j\frac{2\pi\chi Z}{c}} \tag{12}$$

where $X=P\cos\beta_T - Q\cos\beta_R$, $Y=f_{T_{max}}\cos\gamma_T - f_{R_{max}}\cos\gamma_R$, and $Z=D-k_{p'}\delta_T\cos\beta_T+k_{q'}\delta_R\cos\beta_R$, with $P=(p'-p)\,\delta_T/\lambda$, $Q=(q'-q)\,\delta_R/\lambda$, $k_{p'}=(M_T-2p'+1)/2$, and $k_{q'}=(M_R-2q'+1)/2$.

Using (3), (6)–(9), and (11) and considering the von Mises PDF of the AoA and AoD, the STF CF of the two-ring model with single-bounced rays can be expressed as

$$\rho_{h_{pq}^{SB_{1(2)}}h_{p'q'}^{SB_{1(2)}(\dagger)}}(\tau,\chi) = \eta_{SB_{1(2)}}e^{jC_{T(R)}^{SB_{1(2)}}} \times \frac{I_0\left\{\sqrt{\left(A_{T(R)}^{SB_{1(2)}}\right)^2+\left(B_{T(R)}^{SB_{1(2)}}\right)^2}\right\}}{I_0\left(k_{T(R)}^{SB_{1(2)}}\right)} \tag{13}$$

where parameters $A_T^{SB_1}$, $B_T^{SB_1}$, $C_T^{SB_1}$, $A_R^{SB_2}$, $B_R^{SB_2}$, and $C_R^{SB_2}$ are $A_T^{SB_1}=k_T^{SB_1}\cos\mu_T^{SB_1}-j2\pi\tau f_{T_{max}}\cos\gamma_T+j2\pi P\cos\beta_T-j2\pi\chi L_T/c$, $B_T^{SB_1}=k_T^{SB_1}\sin\mu_T^{SB_1}-j2\pi\tau f_{T_{max}}\sin\gamma_T-j2\pi\tau f_{R_{max}}\Delta_T\sin\gamma_R+j2\pi P\sin\beta_T+j2\pi Q\Delta_T\sin\beta_R-j2\pi\chi S_T/c$, $C_T^{SB_1}=2\pi\tau f_{R_{max}}\cos\gamma_R-2\pi Q\cos\beta_R+2\pi\chi T_T/c$, $A_R^{SB_2}=k_R^{SB_2}\cos\mu_R^{SB_2}-j2\pi\tau f_{R_{max}}\cos\gamma_R+j2\pi Q\cos\beta_R-j2\pi\chi L_R/c$, $B_R^{SB_2}=k_R^{SB_2}\sin\mu_R^{SB_2}-j2\pi\tau f_{R_{max}}\sin\gamma_R-j2\pi\tau f_{T_{max}}\Delta_R\sin\gamma_T+j2\pi Q\sin\beta_R+j2\pi P\Delta_R\sin\beta_T-j2\pi\chi S_R/c$, and $C_R^{SB_2}=-2\pi\tau f_{T_{max}}\cos\gamma_T+2\pi P\cos\beta_T+2\pi\chi T_R/c$, with $L_T=R_T+k_{p'}\delta_T\cos\beta_T$, $S_T=k_{p'}\delta_T\sin\beta_T+k_{q'}\delta_R\Delta_T\sin\beta_R$, $T_T=R_T+D+k_{q'}\delta_R\cos\beta_R$, $L_R=-R_R+k_{q'}\delta_R\cos\beta_R$, $S_R=k_{q'}\delta_R\sin\beta_R+k_{p'}\delta_T\Delta_R\sin\beta_T$, $T_R=R_R+D-k_{p'}\delta_T\cos\beta_T$. The symbol $\mu_T^{SB_1}$ $\left(\mu_R^{SB_2}\right)$ denotes the mean value of the AoD $\phi_T^{(n_1)}$ (AoA $\phi_R^{(n_2)}$) and $k_T^{SB_1}$ $\left(k_R^{SB_2}\right)$ controls the angle spread of the AoD $\phi_T^{(n_1)}$ (AoA $\phi_R^{(n_2)}$).

Using (4), (6), (8), (10), and (11) and considering the von Mises PDF of the AoA and AoD, the STF CF of the two-ring model with double-bounced rays can be given by

$$\rho_{h_{pq}^{DB}h_{p'q'}^{DB(\dagger)}}(\tau,\chi) = \eta_{DB}e^{jC^{DB}} \times \frac{I_0\left\{\sqrt{\left(A_T^{DB}\right)^2+\left(B_T^{DB}\right)^2}\right\}I_0\left\{\sqrt{\left(A_R^{DB}\right)^2+\left(B_R^{DB}\right)^2}\right\}}{I_0\left(k_T^{DB}\right)I_0\left(k_R^{DB}\right)} \tag{14}$$

where $C^{DB}=2\pi\chi(R_T+R_R+D)/c$, $A_T^{DB}=k_T^{DB}\cos\mu_T^{DB}-j2\pi\tau f_{T_{max}}\cos\gamma_T+j2\pi P\cos\beta_T-j2\pi\chi k_{p'}\delta_T\cos\beta_T/c$, $B_T^{DB}=k_T^{DB}\sin\mu_T^{DB}-j2\pi\tau f_{T_{max}}\sin\gamma_T+j2\pi P\sin\beta_T-j2\pi\chi k_{p'}\delta_T\sin\beta_T/c$, $A_R^{DB}=k_R^{DB}\cos\mu_R^{DB}-j2\pi\tau f_{R_{max}}\times\cos\gamma_R+j2\pi Q\cos\beta_R-j2\pi\chi k_{q'}\delta_R\cos\beta_R/c$, and $B_R^{DB}=k_R^{DB}\sin\mu_R^{DB}-j2\pi\tau f_{R_{max}}\sin\gamma_R+j2\pi Q\sin\beta_R-j2\pi\chi k_{q'}\delta_R\sin\beta_R/c$, with μ_T^{DB} $\left(\mu_R^{DB}\right)$ denoting the mean value of the AoD $\phi_T^{(n_1)}$ (AoA $\phi_R^{(n_2)}$) and k_T^{DB} $\left(k_R^{DB}\right)$ controlling the angle spread of the AoD $\phi_T^{(n_1)}$ (AoA $\phi_R^{(n_2)}$). Since the derivations of (12)–(14) are similar, only the derivation of (13) is given in Appendix A, while others are omitted here for brevity. Finally, the normalized STF CF between two time-variant complex impulse responses $h_{pq}(t)$ and $h_{p'q'}^{(\dagger)}(t)$ becomes a summation of the STF CFs in (12)–(14), i.e., $\rho_{h_{pq}h_{p'q'}^{(\dagger)}}(\tau,\chi) = \rho_{h_{pq}^{LoS}h_{p'q'}^{LoS(\dagger)}}(\tau,\chi) + \sum_{i=1}^{2}\rho_{h_{pq}^{SB_i}h_{p'q'}^{SB_i(\dagger)}}(\tau,\chi) + \rho_{h_{pq}^{DB}h_{p'q'}^{DB(\dagger)}}(\tau,\chi)$.

The normalized STF CF $\rho_{h_{pq}h_{p'q'}^{(\dagger)}}(\tau,\chi)$ includes many existing CFs as special cases. Assuming the frequency separation $\chi=0$, we can then obtain the CF (18) in [5]. Consequently, the STF CF also includes the CFs listed in [5], e.g., the ones in [3] and [4], as special cases.

B. New Generic SDF PSD

Taking the Fourier transform of the STF CFs in (12)–(14) in terms of time, we can obtain the corresponding SDF PSDs. 1) In terms of the LoS component,

$$F\left\{\rho_{h_{pq}^{LoS}h_{p'q'}^{LoS(\dagger)}}(\tau,\chi)\right\} = \sqrt{K_{pq}K_{p'q'}}e^{j2\pi X + j\frac{2\pi\chi Z}{c}}\delta(f_D+Y) \tag{15}$$

where $\delta(\cdot)$ denotes the Dirac delta function and f_D is the Doppler frequency.

2) In the case of the single-bounced component,

$$F\left\{\rho_{h_{pq}^{SB_{1(2)}}h_{p'q'}^{SB_{1(2)}(\dagger)}}(\tau,\chi)\right\}=\frac{\eta_{SB_{1(2)}}2e^{jU_{T(R)}^{SB_{1(2)}}}}{I_0\left(k_{T(R)}^{SB_{1(2)}}\right)}\times\frac{e^{jO_{T(R)}^{SB_{1(2)}}\frac{D_{T(R)}^{SB_{1(2)}}}{W_{T(R)}^{SB_{1(2)}}}}\cos\left[\frac{E_{T(R)}^{SB_{1(2)}}}{W_{T(R)}^{SB_{1(2)}}}\sqrt{W_{T(R)}^{SB_{1(2)}}-\left(O_{T(R)}^{SB_{1(2)}}\right)^2}\right]}{\sqrt{W_{T(R)}^{SB_{1(2)}}-\left(O_{T(R)}^{SB_{1(2)}}\right)^2}} \tag{16}$$

where $O_T^{SB_1}=2\pi\left(f_D-f_{R_{max}}\cos\gamma_R\right)$, $U_T^{SB_1}=-2\pi Q\cos\beta_R+2\pi\chi\left(R_T+D+k_{q'}\delta_R\cos\beta_R\right)/c$, $W_T^{SB_1}=4\pi^2f_{T_{max}}^2+4\pi^2f_{R_{max}}^2\times\Delta_T^2\sin\gamma_R^2+8\pi^2f_{T_{max}}f_{R_{max}}\Delta_T\sin\gamma_T\sin\gamma_R$, $D_T^{SB_1}=j2\pi k_T^{SB_1}f_{T_{max}}\cos\left(\gamma_T-\mu_T^{SB_1}\right)+j2\pi k_T^{SB_1}f_{R_{max}}\Delta_T\sin\gamma_R\times\sin\mu_T^{SB_1}-4\pi^2Pf_{T_{max}}\cos\left(\beta_T-\gamma_T\right)-4\pi^2Q\Delta_Tf_{T_{max}}\sin\beta_R\times\sin\gamma_T-4\pi^2P\Delta_Tf_{R_{max}}\sin\beta_T\sin\gamma_R-4\pi^2Q\Delta_T^2f_{R_{max}}\sin\beta_R\times\sin\gamma_R+4\pi^2\chi\left(f_{T_{max}}J_1/c+f_{R_{max}}\Delta_T\sin\gamma_RH_1/c\right)$, $E_T^{SB_1}=j2\pi k_T^{SB_1}f_{T_{max}}\sin\left(\gamma_T-\mu_T^{SB_1}\right)+j2\pi k_T^{SB_1}f_{R_{max}}\Delta_T\sin\gamma_R\times\cos\mu_T^{SB_1}+4\pi^2Pf_{T_{max}}\sin\left(\beta_T-\gamma_T\right)+4\pi^2Q\Delta_Tf_{T_{max}}\sin\beta_R\times\cos\gamma_T-4\pi^2P\Delta_Tf_{R_{max}}\cos\beta_T\sin\gamma_R+4\pi^2\chi\left(f_{T_{max}}G_1/c+f_{R_{max}}\Delta_T\sin\gamma_RV_1/c\right)$, $O_R^{SB_2}=2\pi\left(f_D+f_{T_{max}}\cos\gamma_T\right)$, $U_R^{SB_2}=2\pi P\cos\beta_T+2\pi\chi\left(R_R+D-k_{p'}\delta_T\cos\beta_T\right)/c$, $W_R^{SB_2}=4\pi^2f_{R_{max}}^2+4\pi^2f_{T_{max}}^2\Delta_R^2\sin\gamma_T^2+8\pi^2f_{R_{max}}f_{T_{max}}\Delta_R\sin\gamma_R\times\sin\gamma_T$, $D_R^{SB_2}=j2\pi k_R^{SB_2}f_{R_{max}}\cos\left(\gamma_R-\mu_R^{SB_2}\right)+j2\pi\times k_R^{SB_2}f_{T_{max}}\Delta_R\sin\gamma_T\sin\mu_R^{SB_2}-4\pi^2Qf_{R_{max}}\cos\left(\beta_R-\gamma_R\right)-4\pi^2P\Delta_Rf_{R_{max}}\sin\beta_T\sin\gamma_R-4\pi^2Q\Delta_Rf_{T_{max}}\sin\beta_R\sin\gamma_T-4\pi^2P\Delta_R^2f_{T_{max}}\sin\beta_T\sin\gamma_T+4\pi^2\chi\left(f_{R_{max}}J_2/c+f_{T_{max}}\Delta_R\times\sin\gamma_TH_2/c\right)$, $E_R^{SB_2}=j2\pi k_R^{SB_2}f_{R_{max}}\sin\left(\gamma_R-\mu_R^{SB_2}\right)+j2\pi k_R^{SB_2}f_{T_{max}}\Delta_R\sin\gamma_T\cos\mu_R^{SB_2}+4\pi^2Qf_{R_{max}}\sin\left(\beta_R-\gamma_R\right)+4\pi^2P\Delta_Rf_{R_{max}}\sin\beta_T\cos\gamma_R-4\pi^2Q\Delta_Rf_{T_{max}}\times\cos\beta_R\sin\gamma_T+4\pi^2\chi\left(f_{R_{max}}G_2/c+f_{T_{max}}\Delta_R\sin\gamma_TV_2/c\right)$, with $J_1=R_T\cos\gamma_T+k_{p'}\delta_T\cos\left(\beta_T-\gamma_T\right)+k_{q'}\delta_R\Delta_T\sin\beta_R\times\sin\gamma_T$, $H_1=k_{p'}\delta_T\sin\beta_T+k_{q'}\delta_R\Delta_T\sin\beta_R$, $G_1=R_T\sin\gamma_T-k_{p'}\delta_T\sin\left(\beta_T-\gamma_T\right)-k_{q'}\delta_R\Delta_T\sin\beta_R\cos\gamma_T$, $V_1=R_T+k_{p'}\delta_T\cos\beta_T$, $J_2=-R_R\cos\gamma_R+k_{q'}\delta_R\times\cos\left(\beta_R-\gamma_R\right)+k_{p'}\delta_T\Delta_R\sin\beta_T\sin\gamma_R$, $H_2=k_{q'}\delta_R\sin\beta_R+k_{p'}\delta_T\Delta_R\sin\beta_T$, $G_2=-R_R\sin\gamma_R-k_{q'}\delta_R\sin\left(\beta_R-\gamma_R\right)-k_{p'}\delta_T\Delta_R\sin\beta_T\cos\gamma_R$, $V_2=-R_R+k_{q'}\delta_R\cos\beta_R$, $|f_D-f_{R_{max}}\cos\gamma_R|\le\sqrt{W_T^{SB_1}}/(2\pi)$, and $|f_D+f_{T_{max}}\cos\gamma_T|\le\sqrt{W_R^{SB_2}}/(2\pi)$.

3) In terms of the double-bounced component,

$$F\left\{\rho_{h_{pq}^{DB}h_{p'q'}^{DB(\dagger)}}(\tau,\chi)\right\}=\frac{\eta_{DB}e^{jC^{DB}}}{I_0\left(k_T^{DB}\right)I_0\left(k_R^{DB}\right)}\times2e^{j2\pi f\frac{D_T^{DB}}{W_T^{DB}}}\frac{cos\left(\frac{E_T^{DB}}{W_T^{DB}}\sqrt{W_T^{DB}-4\pi^2f^2}\right)}{\sqrt{W_T^{DB}-4\pi^2f^2}}\odot2e^{j2\pi f\frac{D_R^{DB}}{W_R^{DB}}}\frac{cos\left(\frac{E_R^{DB}}{W_R^{DB}}\sqrt{W_R^{DB}-4\pi^2f^2}\right)}{\sqrt{W_R^{DB}-4\pi^2f^2}} \tag{17}$$

where $\odot$ denotes convolution, $D_T^{DB}=-4\pi^2Pf_{T_{max}}\times\cos\left(\beta_T-\gamma_T\right)+j2\pi k_T^{DB}f_{T_{max}}\cos\left(\gamma_T-\mu_T^{DB}\right)+4\pi^2\chi\times f_{T_{max}}k_{p'}\delta_T\cos\left(\beta_T-\gamma_T\right)/c$, $E_T^{DB}=4\pi^2Pf_{T_{max}}\sin\left(\beta_T-\gamma_T\right)+j2\pi k_T^{DB}f_{T_{max}}\sin\left(\gamma_T-\mu_T^{DB}\right)+4\pi^2\chi f_{T_{max}}k_{p'}\delta_T\times\sin\left(\beta_T-\gamma_T\right)/c$, $D_R^{DB}=-4\pi^2Qf_{R_{max}}\cos\left(\beta_R-\gamma_R\right)+j2\pi k_R^{DB}f_{R_{max}}\cos\left(\gamma_R-\mu_R^{DB}\right)+4\pi^2\chi f_{R_{max}}k_{q'}\delta_R\cos\left(\beta_R-\gamma_R\right)/c$, $E_R^{DB}=4\pi^2Qf_{R_{max}}\sin\left(\beta_R-\gamma_R\right)+j2\pi k_R^{DB}f_{R_{max}}\times\sin\left(\gamma_R-\mu_R^{DB}\right)-4\pi^2\chi f_{R_{max}}k_{q'}\delta_R\sin\left(\beta_R-\gamma_R\right)/c$, $W_T^{DB}=4\pi^2f_{T_{max}}^2$, $W_R^{DB}=4\pi^2f_{R_{max}}^2$, and $|f_D|\le\left(\sqrt{W_T^{DB}}+\sqrt{W_R^{DB}}\right)/(2\pi)=f_{T_{max}}+f_{R_{max}}$. Appendix B only gives the derivation of (16), while the derivations of (15)–(17) are similar and therefore are omitted here for brevity. Finally, the SDF PSD between two time-variant complex impulse responses $h_{pq}(t)$ and $h_{p'q'}^{(\dagger)}(t)$ becomes a summation of the SDF PSDs in (15)–(17), i.e., $F\left\{\rho_{h_{pq}h_{p'q'}^{(\dagger)}}(\tau,\chi)\right\}=F\left\{\rho_{h_{pq}^{LoS}h_{p'q'}^{LoS(\dagger)}}(\tau,\chi)\right\}+\sum_{i=1}^{2}F\left\{\rho_{h_{pq}^{SB_i}h_{p'q'}^{SB_{1i}(\dagger)}}(\tau,\chi)\right\}+F\left\{\rho_{h_{pq}^{DB}h_{p'q'}^{DB(\dagger)}}(\tau,\chi)\right\}$.

IV. Numerical Results and Analyses

In this section, based on the derived SDF PSD in Section III, the Doppler PSDs of the two-ring model with single- and double-bounced rays are numerically analyzed in more detail in terms of some important parameters, e.g., the mean values of the AoA and AoD, angle spreads, directions of motion, space separations of antenna elements, and frequency separations. The following parameters are used for our numerical analysis: $f_c=5.9$ GHz, $f_{T_{max}}=f_{R_{max}}=570$ Hz, $D=500$ m, and $R_T=R_R=40$ m.

Fig. 2 shows the influence of single-/double-bounced rays, angle spreads, mean values of the AoA and AoD, and directions of motion on the Doppler PSD. It is clear that in isotropic scattering environments ($k_T=k_R=0$), no matter what the directions of motion are, the Doppler PSD for the single-bounced rays is similar to the U-shape PSD of F2M cellular channels, whereas the PSD for the double-bounced rays has a peak in the middle ("rounded"-shape). We can also observe that the Doppler PSD of the double-bounced rays remains unchanged for different directions of motion, while the Doppler PSD of the single-bounced rays changes according to its position in the normalized Doppler frequency domain keeping the same shape (U-shape). It is worth mentioning that by setting one terminal fixed, our M2M model can reduce to a F2M model. In this case, we restudied the Doppler PSD for either single- or double-bounced rays and found that they have exactly the same U-shape PSD. Due to the limited space of this paper, the results regarding F2M channels are omitted here. These aforementioned observations indicate that the impacts of single- and double-bounced rays on the Doppler PSD are completely different for M2M channels, while they are exactly

the same for F2M channels. Furthermore, it is obvious that the influences of single-bounced rays from different rings (ring around the Tx or Rx) on Doppler PSD are the same for M2M channels when the Tx and Rx move in the parallel and opposite directions. This makes the single-bounced two-ring model have the U-shape Doppler PSD for the parallel and opposite moving directions. When the Tx and Rx move in the same direction, the influences of single-bounced rays from different rings on the Doppler PSD are completely different in terms of the position of the Doppler PSD. Therefore, as shown in Fig. 2, the single-bounced two-ring model has the double-U-shape Doppler PSD for the same moving direction. In such a case, it is desirable to take the different contributions from different rings into account, which were never considered in the existing M2M models, e.g., [5]. Therefore, we can conclude that the more realistic M2M channel model should include the impacts of both single- and double-bounced rays, which implies a new way to construct more accurate M2M channel models. Considering the underlying physical phenomena behind these observations, it seems that the U-shape Doppler PSD will appear in such a scenario that the main received powers are from some large stationary objects (e.g., buildings or bridges) since the AoA and AoD are highly dependent in this case. While the "rounded"-shape Doppler PSD will appear when the main received powers are from some moving objects (e.g., cars around the Tx or Rx) since in this case the AoA and AoD are relatively independent. This conclusion needs to be verified by further measurement results. From Fig. 2, it can be observed that the angle spreads (related to the values of k_T and k_R), mean angles (related to the values of μ_T and μ_R), and directions of motion (related to the values of γ_T and γ_R) significantly affect the behavior of the Doppler PSD. Therefore, these three parameters play an important role in the behavior of the Doppler PSD for non-isotropic scattering environments. Obviously, in an isotropic scattering environment, these impacts vanish.

Figs. 3 and 4 depict the influence of the antenna element spacing and frequency separation on the Doppler PSD, respectively. It is clear that both the space separation and frequency separation introduce fluctuations in the Doppler PSD. It is straightforward to conclude that higher separation (space or frequency) will result in more fluctuations in the Doppler PSD.

V. Conclusions

In this paper, we have derived closed-form STF CFs and the corresponding SDF PSDs for MIMO M2M multicarrier Ricean fading channels in non-isotropic scattering environments based on the two-ring model with single- and double-bounced rays. The novelty of the proposed STF correlation model with derived CFs and PSDs lies in the fact that it considers the impact of the frequency correlation, which has not been studied so far for M2M channels. Based on the derived SDF PSD, we have further investigated the behavior of Doppler PSD in more detail in term of some important parameters. Our numerical evaluations have revealed that the Doppler PSD is very sensitive to the angle spreads, mean values of the AoA and AoD, and directions of motion in non-isotropic scattering environments. The shapes of the Doppler PSD are completely different according to single-bounced rays or double-bounced rays, while they are exactly the same for F2M channels. We have also found that both the spacing and frequency separations introduce fluctuations in the Doppler PSD. It is worth mentioning that these obtained interesting observations and analyses can be considered as useful guidance for further proposing more realistic M2M channel models and setting up future measurement campaigns.

Appendix

A. Derivation of (13)

Considering the von Mises PDF and substituting (3) and (6)–(9) into (11), we have

$$\rho_{h_{pq}^{SB_{1(2)}} h_{p'q'}^{SB_{1(2)}(\dagger)}}(\tau,\chi) = \frac{e^{jC_{T(R)}^{SB_{1(2)}}}}{2\pi I_0\left(k_{T(R)}^{SB_{1(2)}}\right)} \times \int_{-\pi}^{\pi} e^{\left(A_{T(R)}^{SB_{1(2)}}\cos\phi_{T(R)}^{SB_{1(2)}} + B_{T(R)}^{SB_{1(2)}}\sin\phi_{T(R)}^{SB_{1(2)}}\right)} d\phi_{T(R)}^{SB_{1(2)}}. \quad (18)$$

The definite integrals in the right hand side of the above equation can be solved by using the equality $\int_{-\pi}^{\pi} e^{a\sin c + b\cos c} dc = 2\pi I_0\left(\sqrt{a^2+b^2}\right)$ [9]. After some manipulations, we can get the closed-form expression given by (13).

B. Derivation of (16)

Based on mathematical knowledge, we know the equality $a^2 + b^2 = c(d^2 + e^2)$ exists. This allows us to transform $I_0\left[\sqrt{\left(A_{T(R)}^{SB_{1(2)}}\right)^2 + \left(B_{T(R)}^{SB_{1(2)}}\right)^2}\right]$ into the following expression for further derivation

$$I_0\left[j\sqrt{W_{T(R)}^{SB_{1(2)}}} \times \sqrt{\left(\tau + \frac{D_{T(R)}^{SB_{1(2)}}}{W_{T(R)}^{SB_{1(2)}}}\right)^2 + \left(\frac{E_{T(R)}^{SB_{1(2)}}}{W_{T(R)}^{SB_{1(2)}}}\right)^2}\right]. \quad (19)$$

By Fourier transforming (13) in terms of time and using (19) and the equality $\int_0^{\infty} I_0\left(j\alpha\sqrt{x^2+y^2}\right)\cos(\beta x)\,dx = \cos\left(y\sqrt{\alpha^2-\beta^2}\right)/\sqrt{\alpha^2-\beta^2}$ [9], we can obtain the closed-form expression in (16) after some manipulations.

References

[1] A. S. Akki and F. Haber, "A statistical model for mobile-to-mobile land communication channel," *IEEE Trans. Veh. Technol.*, vol. 35, no. 1, pp. 2–10, Feb. 1986.

[2] A. S. Akki, "Statistical properties of mobile-to-mobile land communication channels," *IEEE Trans. Veh. Technol.*, vol. 43, no. 4, pp. 826–831, Nov. 1994.

[3] M. Pätzold, B. O. Hogstad, N. Youssef, and D. Kim, "A MIMO mobile-to-mobile channel model: Part I–the reference model," *Proc. IEEE PIMRC'05*, Berlin, Germany, Sept. 2005, pp. 573–578.

[4] A. G. Zajić and G. L. Stüber, "Space-time correlated MIMO mobile-to-mobile channels," *Proc. IEEE PIMRC'06*, Helsinki, Finland, Sep. 2006, pp.1-5.

[5] A. G. Zajić and G. L. Stüber, "Space-time correlated mobile-to-mobile channels: modelling and simulation," *IEEE Trans. Veh. Technol.*, vol. 57, no. 2, pp. 715–726, Mar. 2008.

[6] C.-X. Wang, M. Pätzold, and Q. Yao, "Stochastic modeling and simulation of frequency correlated wideband fading channels," *IEEE Trans. Veh. Technol.*, vol. 56, no. 3, pp. 1050–1063, May 2007.

[7] X. Cheng, C.-X. Wang, D. I. Laurenson, H. H. Chen, and A. V. Vasilakos, "A generic geometrical-based MIMO mobile-to-mobile channel model," *IEEE IWCMC'08*, Chania Crete Island, Greece, Aug. 2008, accepted for publication.

[8] A. Abdi, J. A. Barger, and M. Kaveh, "A parametric model for the distribution of the angle of arrival and the associated correlation function and power spectrum at the mobile station," *IEEE Trans. Veh. Technol.*, vol. 51, no. 3, pp. 425–434, May 2002.

[9] I. S. Gradshteyn, and I. M. Ryzhik, *Table of Integrals, Series, and Products*. 5th ed, A. Jeffrey, Ed. San Diego, CA: Academic, 1994.

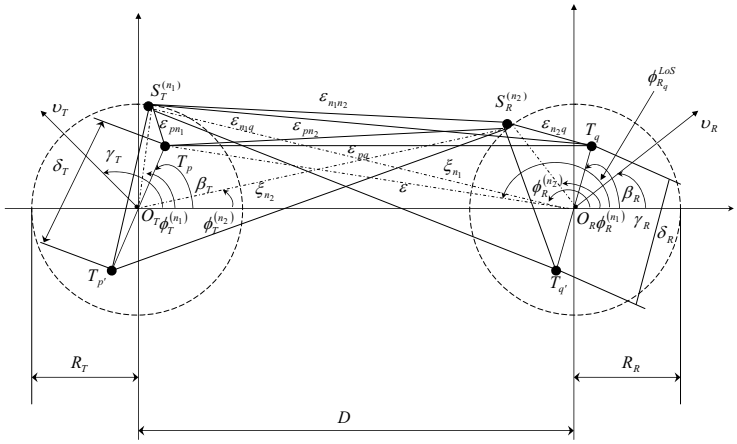

Fig. 1. Two-ring model with the LoS, single-, and double-bounced components for a MIMO M2M channel with $M_T = M_R = 2$ antenna elements.

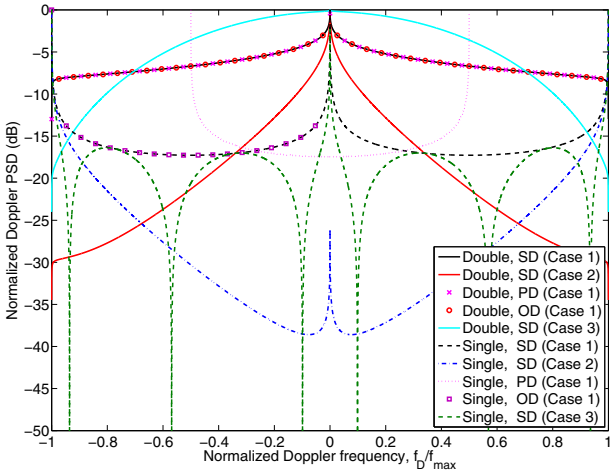

Fig. 2. Normalized Doppler PSDs of the two-ring model with single- and double-bounced rays for different angle spreads, mean angles, and directions of motion ($\delta_T = \delta_R = 0$, $\chi = 0$, and $M_T = M_R = 2$). SD: same direction ($\gamma_T = \gamma_R = 0$); PD: parallel direction ($\gamma_T = \gamma_R = \pi/2$); OD: opposite direction ($\gamma_T = 0$, $\gamma_R = \pi$). Case 1: $k_T = k_R = 0$, $\mu_T = 0$, $\mu_R = \pi$; Case 2: $k_T = k_R = 3$, $\mu_T = 0$, $\mu_R = \pi$; Case 3: $k_T = k_R = 3$, $\mu_T = \mu_R = \pi/2$.

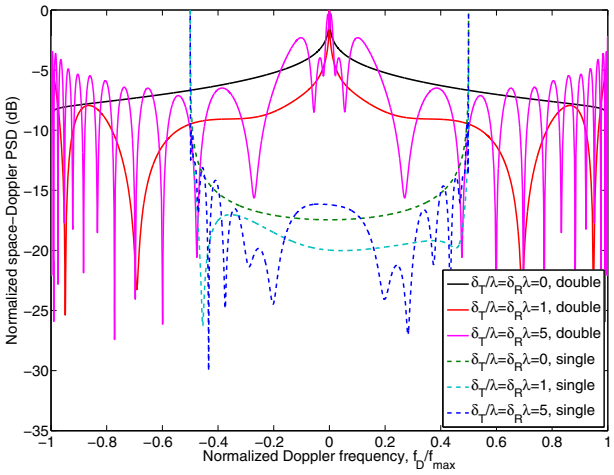

Fig. 3. Normalized Doppler PSDs of the two-ring model with single- and double-bounced rays for different antenna element spacings ($k_T = k_R = 0$, $\chi = 0$, $\mu_T = 0$, $\mu_R = \pi$, $\gamma_T = \gamma_R = \pi/2$, and $M_T = M_R = 2$).

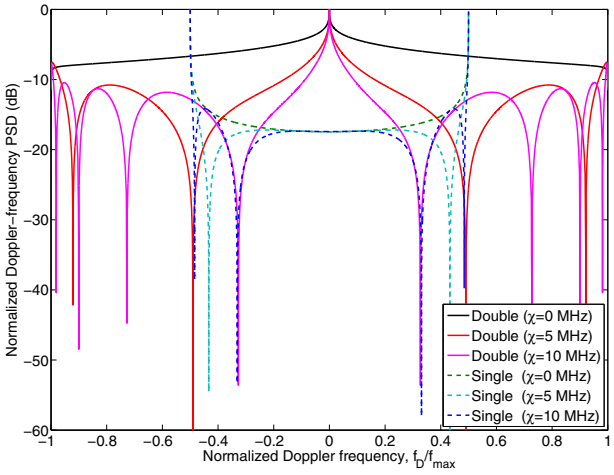

Fig. 4. Normalized Doppler PSDs of the two-ring model with single- and double-bounced rays for different frequency separations ($k_T = k_R = 0$, $\delta_T = \delta_R = 0$, $\mu_T = 0$, $\mu_R = \pi$, $\gamma_T = \gamma_R = \pi/2$, and $M_T = M_R = 2$).